Inorganic Chemistry

ARTICLE

pubs.acs.org/IC

Characterization of Low Energy Charge Transfer Transitions in (terpyridine)(bipyridine)Ruthenium(II) Complexes and their Cyanide-Bridged Bi- and Tri-Metallic Analogues

Chia-Nung Tsai,[‡] Marco M. Allard,[†] Richard L. Lord,[†] Dao-Wen Luo,[§] Yuan-Jang Chen,[*,‡] H. Bernhard Schlegel,[†] and John F. Endicott[*,†]

[†]Department of Chemistry, Wayne State University, Detroit, Michigan 48202, United States

[‡]Department of Chemistry, Fu Jen Catholic University, 510 Chung Cheng Rd Hsinchuang, New Taipei City 24205, Taiwan, R. O. C.

[§]Instruments Center and Department of Chemistry, National Chung-Hsing University, Taichung 402, Taiwan, R. O. C.

Supporting Information

ABSTRACT: The lowest energy metal-to-ligand charge transfer (MLCT) absorption bands found in ambient solutions of a series of $[Ru(tpy)(bpy)X]^{m+}$ complexes (tpy = 2,2′:3′,2″-terpyridine; bpy = 2,2′-bipyridine; and X = a monodentate ancillary ligand) feature one or two partly resolved weak absorptions (bands I and/or II) on the low energy side of their absorption envelopes. Similar features are found for the related cyanide-bridged bi- and trimetallic complexes. However, the weak absorption band I of $[(bpy)_2Ru\{CNRu(tpy)(bpy)\}_2]^{4+}$ is missing in its $[(bpy)_2Ru\{NCRu(tpy)(bpy)\}_2]^{4+}$ linkage isomer demonstrating that this feature arises from a Ru^{II}/tpy MLCT absorption. The energies of the MLCT band I components of the $[Ru(tpy)(bpy)X]^{m+}$ complexes are proportional to the differences between the potentials for the first oxidation and the first reduction waves of the complexes. Time-dependent density functional theory (TD-DFT) computational modeling indicates that these band I components correspond to the highest occupied molecular orbital (HOMO) to lowest unoccupied molecular orbital (LUMO) transition, with the HOMO being largely ruthenium-centered and the LUMO largely tpy-centered. The most intense contribution to a lowest energy MLCT absorption envelope (band III) of these complexes corresponds to the convolution of several orbitally different components, and its absorption maximum has an energy that is about 5000 cm^{-1} higher than that of band I. The multimetallic complexes that contain Ru^{II} centers linked by cyanide have mixed valence excited states in which more than 10% of electronic density is delocalized between the nearest neighbor ruthenium centers, and the corresponding stabilization energy contributions in the excited states are indistinguishable from those of the corresponding ground states. Single crystal X-ray structures and computational modeling indicate that the Ru-(C≡N)-Ru linkage is quite flexible and that there is not an appreciable variation in electronic structure or energy among the conformational isomers.

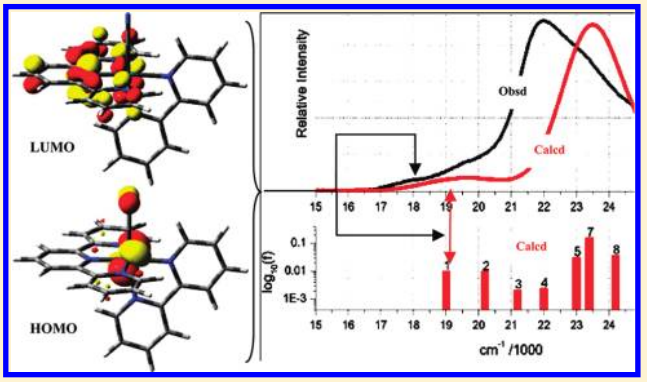

INTRODUCTION

The photoinduced electron-transfer processes of interest in energy conversion and other applications of transition metal complexes generally depend on the lifetimes and reactivities of the lowest energy charge-transfer (CT) excited states. However, the excited state physical properties governing these lifetimes and reactivities are very difficult to establish and, owing to the transient nature of these states, some sort of spectroscopic probing is the most common way to investigate their properties. This is illustrated for absorption or emission spectral probes in an idealized limit in Figure 1. In the simplest limit, the metal to ligand charge transfer (MLCT) excited states generated by absorption, and those whose emission is observed, have the same orbital occupations but differ in their spin multiplicities: either singlet ^{1}MLCT or triplet ^{3}MLCT, respectively.

The excited state initially generated by light absorption (the Franck−Condon excited state, $^1MLCT_{FC}$) has the ground state nuclear coordinates, and the distortions at its potential energy (PE) minimum can sometimes be inferred from resonance-Raman (rR) spectra.[1−5] The ^{1}MLCT→^{3}MLCT intersystem crossing often falls into the subps regime for transition metal complexes,[6] so that the lowest energy excited states tend to be responsible for most of their photoinduced chemistry. The excited state energy and the differences between reactant and product nuclear coordinates tend to determine reactivity patterns.[7,8] In the simplest cases the excited state nuclear coordinates would be largely associated with changes in orbital occupation and in principle the structures of electronically excited systems could be experimentally probed by means of absorption (^{1}MLCT) and/or emission (^{3}MLCT) spectroscopy. Such experimental probing of excited states can be usefully

Received: May 24, 2011
Published: November 08, 2011

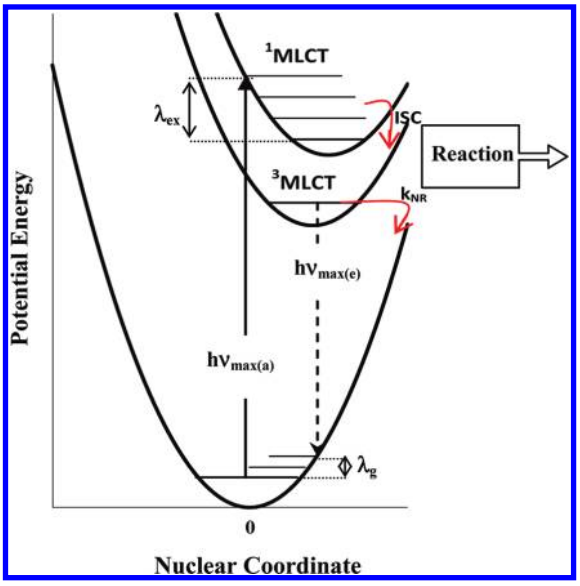

Figure 1. Qualitative representation of the processes characteristic of a simple photosystem system with a single donor (metal) and a single acceptor (ligand). Abbreviations: a, absorption; e, emission; ISC, intersystem crossing; NR, nonradiative relaxation; MLCT, metal to ligand charge transfer; G, ground state; λ_{ex} and λ_g are the excited state and ground state reorganizational energies, respectively.

complemented by computational modeling. However, real transition metal complexes are rarely appropriately represented by very simple limits. Thus, CT absorption spectra can be difficult to assign since: (a) weak shoulders that are apparently of charge transfer origin have been observed for several complexes on the low energy sides of their lowest energy MLCT absorption "bands";[9−11] and (b) computational modeling has indicated that the lowest energy transitions involving the highest occupied molecular orbital (HOMO) and lowest unoccupied molecular orbital (LUMO) can have very small oscillator strengths.[12−15] As a consequence, the dominant absorption spectral features sometimes probe the higher energy excited states and this can be a problem in attempting to characterize the reaction patterns of the lowest energy MLCT excited states since the nuclear distortions of the different ^{1}MLCT and/or ^{3}MLCT excited states are not likely to be the same. Insight into the nuclear distortions of the lowest energy ^{3}MLCT excited states can often be obtained from emission spectroscopy and this is an area of continuing study,[11,16−20] while computational modeling of these vibrationally relaxed, open shell electronic excited states has been more difficult than that of their Franck−Condon excited states. Thus, the information that can be gleaned from absorption spectroscopy can be very useful in determining the limits and general patterns of the variations in the energies and structures of the lowest energy excited states.

While the identification of the absorption band corresponding to the lowest energy MLCT excited state might provide useful information about excited state reactivity, recent studies of series of $[Ru(L)_{6-2n}(bpy)_n]^{m+}$ complexes (n = 1,2) have shown that the experimental identification of the MLCT absorption corresponding to the lowest energy excited state (corresponding to the HOMO→LUMO transition) in such electron rich transition metal complexes with electron acceptor ligands (A) are especially difficult because of the following:[13] (a) there are typically several nearly degenerate donor (D) orbitals (e.g., three for a low spin d^6 metal in an O_h environment); (b) the other coordinated, or ancillary ligands affect both the energies and spatial orientations of the donor orbitals thereby altering the D/A spatial overlap and the observed absorptivity.

The $[Ru(tpy)(bpy)L]^{m+}$ and $[Ru(bpy)_2L_2]^{m+}$ complexes are in principle closely related to electron-transfer systems with a single donor center and two acceptor centers, and the contrast between the different acceptors of the former and identical acceptors of the latter is expected to result in appreciable contrasts in the nature and properties of the respective lowest energy MLCT excited states. Furthermore, the electronic structures of the $[Ru(tpy)(bpy)L]^{m+}$ complexes are of more general importance because of interest in their reactivity as oxidation catalysts.[21−23] The absorption spectra of these complexes exhibit weak low energy features somewhat analogous to their bis-bpy analogues, but these low energy absorption shoulders extend over a larger energy range. Obviously, some of the spectroscopic differences in the two classes of complexes must arise from the differences in the acceptor moieties, but both classes of complexes are of the DA_2 type and the HOMO→LUMO transitions of DA_2 complexes often have small oscillator strengths[12−15] which are difficult to identify in experimental spectra. Thus, the HOMO→LUMO transitions could contribute to the low energy shoulders of the $[Ru(tpy)(bpy)L]^{m+}$ complexes. The present report uses differences in the low energy MLCT spectra of the linkage isomers of cyanide-bridged triruthenium complexes, spectral/electrochemical correlations, and time-dependent density functional theory (TD-DFT) modeling to demonstrate that it is these relatively weak, lowest energy absorption features of $[Ru(tpy)(bpy)L]^{m+}$ complexes that are associated with the Ru^{II}/tpy HOMO→LUMO transition for monometallic and some related cyanide-bridged bi- and trimetallic complexes.

EXPERIMENTAL SECTION

1. Materials and Synthesis of Compounds. The following commercial chemicals were used with no further purification: $RuCl_3 \cdot 3H_2O$, 2, 2′-bipyridine, 2,2′:6′,2″-terpyridine, NaCN, NH_4OH, CH_3CN, pyridine, pyrazine, (Aldrich); NH_4I, KPF_6 (SHOWA), NH_4PF_6 (STREM). Literature syntheses were used for the following compounds: $[Ru(tpy)(bpy)(Cl)]Cl$,[24] $[Ru(tpy)(bpy)I](PF_6)$,[25] $[Ru(tpy)(bpy)(CN)](PF_6)$,[26] $[Ru(tpy)(bpy)(NH_3)](PF_6)_2$,[27] $[Ru(tpy)(bpy)(NCCH_3)](PF_6)_2$,[28] $[Ru(tpy)(bpy)(py)](PF_6)_2$,[28] and $[Ru(tpy)(bpy)(pz)](PF_6)_2$.[29]

[Ru(tpy)(bpy)(Br)](PF$_6$). A mixture of $[Ru(tpy)(OTF)_3]$ (256.97 mg, 0.333 mmol), 2,2′-bipyridine (54.73 mg, 0.35 mmol), NaBr (67.62 mg, 0.66 mmol), and 75 mL of ethanol was refluxed for 24 h in an argon atmosphere, then injected into a 1.5 mL saturated aqueous NH_4PF_6 solution and cooled. After 2 h, the solution was filtered to obtain the crude product. This was purified by chromatography using aluminum oxide 90 active neutral (Merck) as the stationary phase, and a mixture of CH_3CN/toluene (1:3 (v/v)) as the eluent. The second band was collected, and the solvent removed by rotary evaporation. Finally, this sample was vacuum-dried to obtain the product(125 mg, 0.15 mmol). The typical yield was 44%. Anal. Calcd (found) for $C_{25}H_{19}N_5BrF_6PRu$: C, 41.97 (41.89); H, 2.68 (2.95); N, 9.79 (9.43).

[{(tpy)(bpy)Ru}$_2$CN](PF$_6$)$_3$. A solution containing $[Ru(tpy)(bpy)Cl]Cl$ (103 mg, 0.183 mmol), $[Ru(tpy)(bpy)(CN)](PF_6)$ (104 mg, 0.157 mmol), and H_2O (60 mL) was refluxed for 4 days in an argon atmosphere. As this solution began to cool it was combined with 5 mL of a saturated aqueous KPF_6 solution. After 3 h, the solution was filtered to obtain the crude product. The product was further purified chromatographically as above, and the second band was collected and the solvent removed by rotary evaporation. Finally, this sample was vacuum-dried to

dx.doi.org/10.1021/ic2010387 |*Inorg. Chem.* 2011, 50, 11965–11977

Table 1. Absorption Spectra and the Electrochemistry of $[Ru(tpy)(bpy)X]^{m+}$ Complexes

	$E_{1/2}$,[a] V			$h\nu_{max}$(abs; MLCT), cm^{-1} (ε_{max}, M^{-1} cm^{-1}/1000)	
complexes [(L) = (tpy)(bpy)]	$Ru^{III/II}$	$tpy^{0/1-}$ [b]	$F\Delta E_{1/2}$(Ru/tpy)[c]	band I [II][d]	band III[e]
$[Ru(L)Cl]^{+}$	0.861	−1.37 [f]	18,000	15,100 (0.2),	20,000 (5.7)
	(0.845)	(−1.39)		[16,400 (0.6)]	
$[Ru(L)Br]^{+}$	0.888	−1.40 [f]	18,500	15,600 (0.9)	20,000 (10.1)
	(0.870)	(−1.34)		[16,800 (1.1)]	
$[Ru(L)I]^{+}$	0.895	−1.30 [f]	17,700	15,600(0.7),	19,900 (8.9)
	(0.870)	(−1.32)		[17,000(1.2)]	
$[Ru(L)CN)]^{2+}$	1.135	−1.321	19,810	16,400 (0.5),	20,600 (12.0)
	(1.124)	(−1.296)		[18,700 (2.3)]	
$[Ru(L)(NH_3)]^{2+}$	1.139	−1.259	19,340	16,400 (0.5),	20,800 (7.2)
	(1.112)			[17,600 (0.8)]	
$[Ru(L)py)]^{2+}$	1.288	−1.191	20,000	17,100 (0.7),	21,500 (9.0)
	(1.260)			[18,500 (1.0)]	
$[Ru(L)pz)]^{2+}$	1.378	−1.148	20,370	17,500 (0.4)	22,200 (13.5)
	(1.364)	(−1.128)		[18,900 (1.2)]	
$[Ru(L)NCCH_3)]^{2+}$	1.366	−1.225	20,900	18,300 (0.4),	22,100 (7.2)
	(1.344)			[19,600 (0.7)]	
$[(L)Ru\text{-}\{CNRu(L)\}]^{3+}$	1.502	−1.327	19,360	16,300 (0.3),	21,600 (14.4)
	1.070 [g]			[17,600 (1.1)]	
$[(L)Rh\text{-}\{CNRu(L)\}]^{4+}$ [h]	1.148	[−1.261][i]	[(19,430)][j]	16,700 (1.3),	20.6 (17.7)
	(1.124)	[(−1.238)][i]		[18,000 (1.9)]	
$[(bpy)_2Ru\text{-}\{CNRu(L)\}_2]^{4+}$	1.820	−1.317	18,750	16,200 (1.2),	21,550 (24.6)
	1.137			[17,300 (0.9)]	
	1.008				
$[(bpy)_2Ru\text{-}\{NCRu(L)\}_2]^{4+}$	1.564	−1.295	17,520[k]	16,800 (1.4)	22,000 (20.7)
	1.433		18,600[l]	[18,300 (1.5)]	
	0.877				
$[(bpy)_2Rh\text{-}\{CNRu(L)\}_2]^{5+}$ [h]	1.361	[−1.289][i]	[(21,370)][j]	17,500 (1.1),	21,800 (17.2)
				[18,900 (1.4)]	

[a] In MeCN 0.1 M $[n\text{-}Bu_4N]PF_6$, sweep rate 0.1 V s^{-1}, and recorded at room temperature; $E_{1/2}$ values in volts vs Ag/AgCl (3 M NaCl, BAS-RE5B). DPV values in parentheses. [b] First reduction wave. [c] Value in cm^{-1} based on differences in halfwave potentials. [d] Lowest energy CT absorptions for Ru^{II} complexes (band I upper and band II lower entry); component Gaussian peaks deconvoluted from the experimental spectrum using Igor Pro. [e] Maximum of dominant low energy MLCT absorption. [f] First reduction Irreversible wave approximate half-wave potential. [g] Values of 1.41 and 1.00 V were found previously for the oxidations of this complex in acetonitrile with 0.1 M $[Et_4N]PF_6$ and a ferrocene/ferrocenium internal reference.[30] [h] The $Rh^{III/II}$ reduction is irreversible between −0.80 V and −0.945 in the CV scans, see Supporting Information. [i] Since the products of Rh^{III} reduction are not known, this may not correspond to the potential for reduction of tpy in the parent complex. [j] An estimate assuming that the reduction potential of tpy in the parent complex is the same as the value in the preceding column. [k] For $(bpy)_2Ru^{II}$ to the remote tpy ligand. [l] For $(tpy)(bpy)Ru^{II}$ to the coordinated tpy ligand in a $(tpy)(bpy)Ru^{II}(C{\equiv}N)Ru^{III}(bpy)_2$ mixed valence complex.

obtain the product (127 mg, 0.088 mmol). The typical yield was 56%. Anal. Calcd (found) for $C_{51}H_{38}N_{11}F_{18}P_3Ru_2\cdot(C_7H_8)$: C, 45.33 (45.07); H, 3.02 (3.24); N, 10.03 (9.75). This complex has also been prepared by a similar procedure using $[Ru(tpy)(bpy)O_3SCF_3]CF_3SO_3$ rather than the chloride complex.[30]

[(bpy)$_2$Ru{CNRu(tpy)(bpy)}$_2$](PF$_6$)$_4$. A mixture of $[Ru(bpy)_2(CN)_2]\text{-}(H_2O)_2$ (22 mg, 0.044 mmol) and [Ru(tpy)(bpy)Cl]Cl (53 mg, 0.094 mmol) in H_2O (31 mL) was refluxed for 4 days in an Ar atmosphere. Then, saturated aqueous NH_4PF_6 (2 mL) was injected into a round-bottom flask and the mixture was chilled to precipitate the target complex, $[(bpy)_2Ru\{(CN)\text{-}Ru(tpy)(bpy)\}_2](PF_6)_4$. All steps of the synthesis were carried out in an argon atmosphere. The sample was purified chromatographically twice following the procedure described above. The second brown band of the second chromatographic purification contained the desired compound. The solvent was removed by rotary evaporation followed by drying in vacuum. The typical yield was 36% (32 mg; 0.016 mmol). Anal. Calcd (found) for $C_{72}H_{54}N_{16}F_{24}P_4Ru_3$: C, 42.60 (42.88); H, 2.68 (2.71); N, 11.04 (10.97).

[(tpy)(bpy)Rh{CNRu(tpy)(bpy)}](PF$_6$)$_4\cdot$(CH$_3$CN)$_2$. A mixture of 356.6 mg (0.44 mmol) of $[Rh(tpy)(bpy)Cl](PF_6)_2$ and 23.5 mg (0.48 mmol) of NaCN in 45 mL H_2O was refluxed for 24 hours then combined with 2mL of saturated aqueous NH_4PF_6 and the mixture was chilled to precipitate the target complex. After 30 minutes the mixture was filtered to obtain $[Rh(tpy)(bpy)CN](PF_6)_2$. An aqueous solution (45 mL) containing 68 mg (0.12 mmol) [Ru(tpy)(bpy)Cl]Cl and 74 mg (0.09 mmol) $[Rh(tpy)(bpy)(CN)](PF_6)_2$ was refluxed for 4 days in an argon atmosphere then combined with 1.5 mL saturated aqueous NH_4PF_6. The solution was cooled for 3 hrs, and the cold solution was filtered to obtain the crude product. The product was purified chromatographically as above. The second band was collected and the solvent removed by rotary evaporation. The solid residue was vacuum-dried to obtain a 73 mg (0.05 mmol) of the product. The typical yield was 56 %. The pure product (needle crystal) was obtained by slow diffusion of ether into a saturated CH_3CN solution containing the crude product. Anal. Calcd (found) for $C_{55}H_{44}N_{13}F_{24}P_4RhRu$: C, 39.54 (39.45); H, 2.65 (3.12); N, 10.90 (10.97).

dx.doi.org/10.1021/ic2010387 |*Inorg. Chem.* 2011, 50, 11965–11977

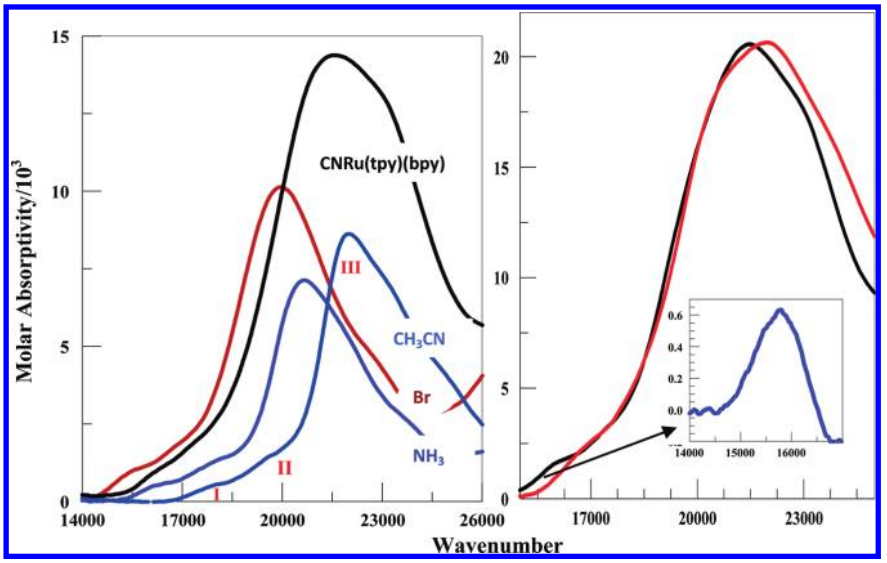

Figure 2. Lowest energy MLCT absorption envelopes of selected $[Ru(tpy)(bpy)X]^{m+}$ complexes, left panel (X indicated on the curves in the panel); note that the black curve is for the bimetallic complex. The lowest energy MLCT spectra of the $[(bpy)_2Ru\{CNRu(tpy)(bpy)\}_2]^{4+}$ (black curve) and $[(bpy)_2Ru\{NCRu(tpy)(bpy)\}_2]^{4+}$ (red curve) complexes are compared in the right panel. Inset is the difference between the $[(bpy)_2Ru\{CNRu(tpy)(bpy)\}_2]^{4+}$ and $[(bpy)_2Ru\{NCRu(tpy)(bpy)\}_2]^{4+}$ spectra in the 14,000−17,000 cm^{-1} region. Bands I, II, and III of the lowest energy MLCT absorption envelope are indicated in the left panel for $[Ru(tpy)(bpy)CH_3CN]^{2+}$.

$[(bpy)_2Ru\{NC\text{-}Ru(tpy)(bpy)\}_2](PF_6)_4$. A solution of mg (0.278 mmol) $[Ru(tpy)(bpy)(CN)](PF_6)$ and 74.14 mg (0.142 mmol) $Ru(bpy)_2Cl_2\cdot 2H_2O$ in 95 mL H_2O was refluxed under argon for 4 days. A 6 mL half-saturated aqueous solution of NH_4PF_6 was added to the reaction mixture at room temperature. The crude brown product that resulted was then filtered. The complex was purified by chromatographically as above, the second band was collected and the solvent was removed by the rotary evaporation. The typical yield was 37%. Anal. Calcd (found) for $C_{72}H_{54}N_{16}F_{24}P_4Ru_3$: C, 42.60 (42.05); H, 2.68 (2.57); N, 11.04 (11.30).

$[(bpy)_2Ru\{NCRu(tpy)(bpy)\}_2](PF_6)_4$. A mixture of of $[Ru(bpy)_2(CN)_2](H_2O)_2$ (22 mg, 0.044 mmol) and $[Ru(tpy)(bpy)Cl]Cl$ (53 mg, 0.094 mmol) in H_2O (31 mL) was refluxed under argon for 4 days. Then saturated aqueous NH_4PF_6 (2 mL) was injected into a round-bottom flask containing the reaction mixture under Ar at room temperature, and this mixture was chilled to form the precipitate of $[(bpy)_2Ru\{CNRu(tpy)(bpy)\}_2](PF_6)_4$. The crude brown product that resulted was then filtered and purified twice by column chromatography as above. The second brown band of the second purification contained the desired compound, and the solvent was removed by rotary evaporation followed by drying in vacuum. The typical yield was 36% (32 mg; 0.016 mmol). Anal. Calcd (found) for $C_{72}H_{54}N_{16}F_{24}P_4Ru_3$: C, 42.60 (42.05); H, 2.68 (2.57); N, 11.04 (11.30).

$[(bpy)_2Rh\{CNRu(tpy)(bpy)\}_2](PF_6)_5\cdot(H_2O)_2$. A sample containing $[Rh(bpy)_2(CN)_2](PF_6)$ (30.56 mg, 0.047 mmol) and $[Ru(tpy)(bpy)Cl]Cl$ (57.77 mg, 0.103 mmol) was refluxed in H_2O (20 mL) for 4 days. A portion of saturated aqueous KPF_6 (3 mL) was added to the solution, then it was cooled to room temperature, and crude product was filtered. This whole procedure was carried out under an argon atmosphere. The crude product was purified by chromatography as above. The typical yield was 20%. Anal. Calcd (found) for $C_{72}H_{58}N_{16}F_{30}O_2P_5Rh_1Ru_2$: C, 39.14 (38.57); H, 2.65 (2.68); N, 10.14 (10.23).

2. Absorption Spectroscopy (UV−vis−NIR). UV−vis−NIR Absorption Spectra of these metal complexes in the solution of acetonitrile were determined with a Shimadzu UV-3101PC or UV-2101PC spectrophotometer at 298 K.

Deconvolutions of the lowest energy observed MLCT absorption bands were performed using the multipeak 2.0 routine in the IGOR Pro 6.2.1.0 program.[31] The observed absorption spectra, I_{obsd}, have been deconvoluted without the frequency correction ($I_{corr} = I_{obsd} \times \nu_m$) where ν_m is the measured frequency. This correction may make about a 5% difference in the $(h\nu_{II} - h\nu_I)$ values in Table 1 below, but this is within the estimated deconvolution and other experimental uncertainties. It is important to note that the Gaussian deconvolutions and TD-DFT modeling approaches that we have used do not include any estimate of vibronic sideband contributions while resonance-Raman spectra indicate that these can constitute an appreciable contribution for absorption spectra.[3−5]

3. Electrochemistry. Electrochemical measurements were performed using an Epsilon Electrochemical Workstation. Cyclic voltammograms (CV) and differential pulse voltammograms (DPV) were obtained in acetonitrile solution, which contained 10^{-3} M complex and 0.1 M $[n\text{-}Bu_4N]PF_6$ at scan rates of 100 mV/s and 4 mV/s, respectively. A three-electrode system consisting of a Pt-disk (1 mm) working electrode (polished with 0.1−0.3 μm Baikowski alumina suspension), a Pt-wire counter electrode, and a Ag/AgCl (3 M NaCl; BAS RE-5B) reference electrode was used. The half-wave potential of ferrocene has been reported as 0.43 V vs Ag/AgCl (3 M NaCl) in acetonitrile,[32] and 0.367 V vs SSCE in acetonitrile.[33,34] We have used $E_{1/2}(Fc^{+1,0}) = 0.437 \pm 0.005$ V vs Ag/AgCl in acetonitrile as the internal standard.

4. X-ray Crystallography. Single crystals were obtained by slow diffusion of ether into a saturated CH_3CN solution containing $[Ru(tpy)(bpy)CN](PF_6)$ or $[Ru\text{-}CN\text{-}Ru](PF_6)_3$. Diffraction data were measured using an Oxford diffraction Geminis S diffractometer with Mo radiation. Cell parameters were determined from 6007 reflections (R(int) = 0.0397) in the range of $5.80° \le 2\theta \le 58.38°$ for $[Ru(tpy)(bpy)CN](PF_6)$, and from 13373 (R(int) = 0.0224) reflections in the range of $5.22° \le 2\theta \le 58.31°$ for $[\{(tpy)(bpy)Ru\}_2CN](PF_6)_3$.The crystal structures of $[Ru(tpy)(bpy)I](PF_6)$, $[Ru(tpy)(bpy)CN](PF_6)$, or $[\{(tpy)(bpy)Ru\}_2CN](PF_6)_3$ were solved and refined using the Bruker SHELXTL-97.[35] Summaries of the crystallographic parameters $[Ru(tpy)(bpy)CN](PF_6)$, and $[\{(tpy)(bpy)Ru\}_2CN](PF_6)_3$ and the ORTEP drawing of $[Ru(tpy)(bpy)CN](PF_6)\cdot(CH_3CN)\cdot(H_2O)_{0.5}$ and $[\{(tpy)(bpy)Ru\}_2CN](PF_6)_3\cdot(CH_3CN)_2$ are shown in the Supporting Information, Tables S1a and S1b.[36]

5. Computational Details. Electronic structure calculations were carried out using DFT[37] as implemented in a development version of Gaussian.[38] In a previous report on the absorption spectra of related

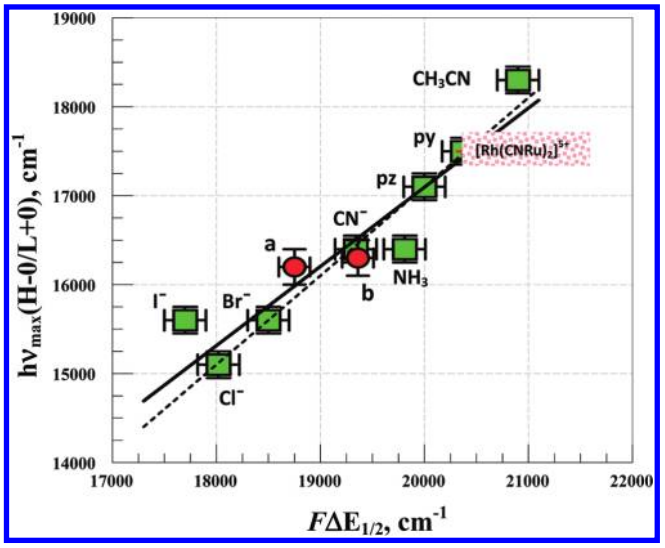

Figure 3. Correlation of the deconvoluted band I energy maxima of the $[Ru(tpy)(bpy)L]^{m+}$ complexes with the differences in the first oxidation and the first reduction half-wave potentials: monometallic complexes (L indicated in figure), green squares; red circles for $[(bpy)_2Ru\{CNRu(tpy)(bpy)\}_2]^{4+}$ (a) and $[\{(tpy)(bpy)Ru\}_2CN]^{3+}$ (b); light red rectangle for $[(bpy)_2Rh\{CNRu(tpy)(bpy)\}_2]^{5+}$ (complex decomposition following Rh^{III} reduction leads to the uncertainty in $E_{1/2}(tpy/tpy^-)$). The dashed line is drawn with a slope of 1.00 and an intercept of -2200 cm^{-1}. The error bars correspond to estimated uncertainties of ± 200 cm^{-1} in $h\nu_{max}$(H-0/L+0) and ± 150 cm^{-1} in $F\Delta E_{1/2}$.

$[(bpy)_2Ru(L)_2]^{n+}$ complexes,[13] we tested a number of modeling approaches and found that the B3PW91 functional[39−42] in combination with the SDDall basis set[43−45] produced good correlation with experiment for a modest cost. Wave functions were tested for SCF stability[46,47] and all optimized structures were confirmed as minima by analyzing the harmonic vibrational frequencies.[48] Solvation effects (in acetonitrile) were accounted for using the most recent implementation of the implicit IEF-PCM solvation model.[49−52] Vertical electronic excitation energies and intensities were evaluated using TD-DFT,[53−55] the resultant plots were generated using SWizard,[56] and isodensity plots of the orbitals involved in these transitions were visualized using GaussView.[57]

Since there was uncertainty about the electrochemistry of $[Ru(tpy)(bpy)X]^+$ for several halides, we evaluated the redox potentials for the monometallic complexes using DFT.[58,59] To generate the computed redox potentials, oxidized and reduced doublet species have been optimized in addition to the ground state singlet. All of these optimizations included an implicit solvation reaction field since DFT overemphasizes charge delocalization because of the self-interaction error.[60] Others have shown the reduced or charge transfer states in Ru species with more than one polypyridyl acceptor can be properly localized by using a suitable model for solvation.[61] Additional single point calculations were performed replacing the SDD basis on the main-group elements (except I) with 6-311+G(d,p). Both sets of data employed thermal corrections obtained at the lower level of theory. The free energy difference associated with a given oxidation or reduction was obtained through eq 1, and converted to an absolute potential with eq 2:

$$\Delta G(\mathrm{Sol})^{\mathrm{redox}} = G(\mathrm{Sol})^{n} - G(\mathrm{Sol})^{n+1} \quad (1)$$

$$E^{\circ}_{\mathrm{comp}} = -\Delta G(\mathrm{Sol})^{\mathrm{redox}}/nF \quad (2)$$

where $G(\mathrm{sol})^{X}$ is the solution-phase free energy for the species with charge X; $\Delta G(\mathrm{Sol})^{\mathrm{redox}}$ is the solution-phase free energy difference for a given redox event (written as a reduction); $E^{\circ}_{\mathrm{comp}}$ is the computed absolute potential related with that redox event. Normally one converts the absolute potentials to relative potentials using experimental or empirical conversion factors,[59] but we omit this step because we are only interested in the difference between the $Ru^{III/II}$ and $tpy^{0/1-}$ potentials which is independent of the reference potential.

For the diruthenium species, the lowest energy TD-DFT calculated transition was not HOMO→LUMO. To unambiguously assign the donor/acceptor pair for the lowest energy MLCT excited state, natural transition orbitals (NTOs) were computed as has been done in related studies on mononuclear $[(bpy)(tpy)RuL]^{n+}$ complexes.[62,63]

RESULTS

A. Absorption Spectra and Electrochemistry. All of the complexes discussed here have relatively intense shoulders on the low energy side of their dominant MLCT absorption bands with one or two partially resolved absorption contributions (bands I and II); Figures 2 and Supporting Information, Figure S2.[36] The deconvoluted low energy absorption features and the absorption spectra and electrochemical observations are summarized in Table 1. The multi-Ru complexes other than $[(bpy)_2Rh\{CNRu(tpy)(bpy)\}_2]^{5+}$ develop low energy, metal-to-metal CT (MMCT) absorption bands upon oxidation as summarized in Supporting Information, Table S3 and Figure S3.[36]

The low energy MLCT absorption envelopes of the linkage isomers $[(bpy)_2Ru\{CNRu(tpy)(bpy)\}_2]^{4+}$ and $[(bpy)_2Ru\{NCRu(tpy)(bpy)\}_2]^{4+}$ are very similar, as shown in the right panel of Figure 2, with the major differences attributable to the oxidation potentials for Ru^{II}/Ru^{III} couples with different linkages to cyanide (Ru−C or Ru−N). Thus, the $Ru^{II}(-CN)_2$ centers are harder to oxidize than the $Ru^{II}(-NC)_2$ centers by 400−700 mV (Table 1) whereas the reductions of the coordinated tpy ligand are less than 270 mV more positive than those of the coordinated bpy ligand; this pattern is also observed in the calculated orbital energies. As a consequence, the lowest energy MLCT absorption band of $[(bpy)_2Ru\{CNRu(tpy)(bpy)_2]^{4+}$ is expected to be a Ru^{II}/tpy MLCT transition involving the (tpy)(bpy)Ru(−NC) centers but the corresponding absorption of $[(bpy)_2Ru\{NCRu(tpy)(bpy)\}_2]^{4+}$ should occur at appreciably higher energy. For these reasons, the stronger absorption of $[(bpy)_2Ru\{CNRu(tpy)(bpy)\}_2]^{4+}$ than $[(bpy)_2Ru\{NCRu(tpy)(bpy)\}_2]^{4+}$ in the 14,000−17,000 cm^{-1} region (band I) is attributed to a Ru^{II}/tpy MLCT transition which occurs with a larger absorptivity and at a lower energy in the former. The maximum of the Ru^{II}/tpy MLCT peak in the inset is at 15,800 cm^{-1} which compares well with the 16,200 cm^{-1} estimate based on the IGOR deconvolution (Table 1). This comparison of the spectra of the linkage isomers of cyanide-bridged tri-Ru^{II} complexes nicely demonstrates that band I is a weak Ru^{II} /tpy MLCT absorption band.

The first oxidation and the first reduction waves (corresponding to the metal centered oxidations and the tpy ligand centered reductions, respectively) of the $[Ru(tpy)(bpy)X]^+$ complexes were well behaved: (a) these oxidation and reduction waves had similar amplitudes in both the CV and the DPV modes; and (b) there was less than 90 mV peak-to-peak separations between the anodic and the cathodic CV components of either the oxidation or the reduction waves, except for the complexes with X = halide. The reduction wave for the halide complexes was misshaped while the oxidations were generally complicated by catalytic waves at relatively high potentials (≈ 2 V; Supporting Information, Figure S4).[36] Consequently we have computationally modeled the first oxidations and reductions of

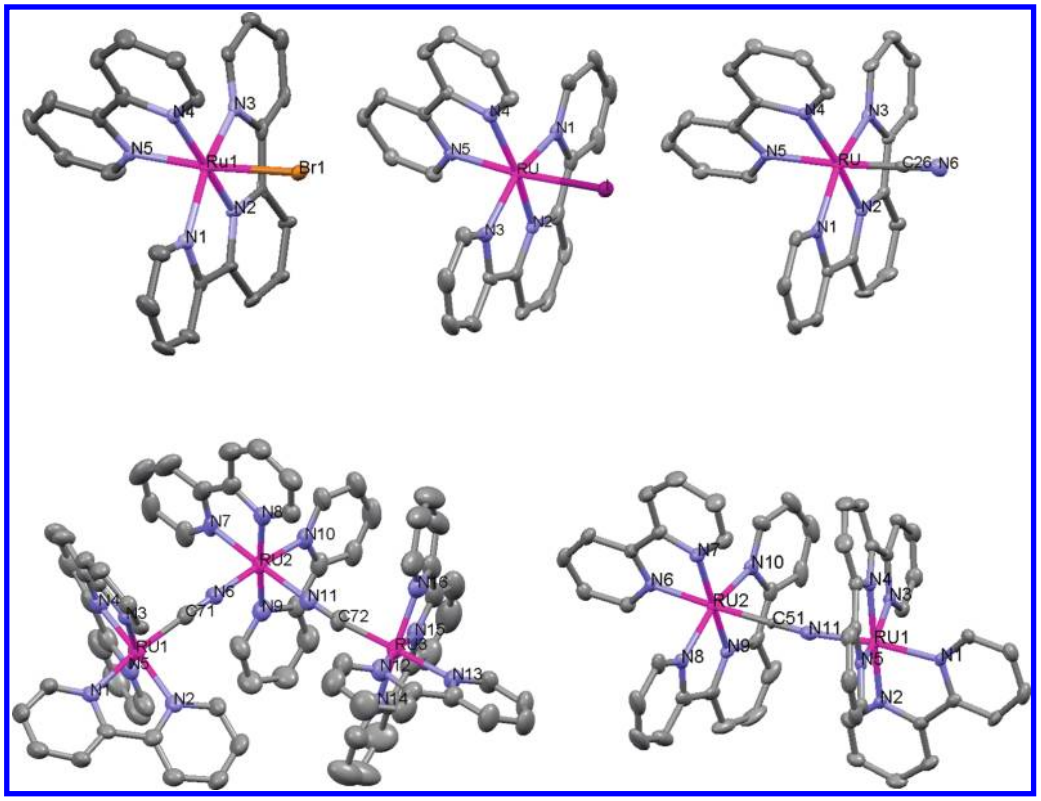

Figure 4. X-ray structures of $[Ru(tpy)(bpy)Br](PF_6)\cdot(C_4H_{10}O)_{0.5}$, left top; $[Ru(tpy)(bpy)I](PF_6)$, central top;, $[Ru(tpy)(bpy)CN](PF_6)\cdot(CH_3CN)\cdot(H_2O)_{0.5}$, right top; $[\{Ru(bpy)(tpy)\}_2CN](PF_6)_3\cdot(CH_3CN)_2$ and $[Ru(bpy)_2\{NCRu(bpy)(tpy)\}_2](PF_6)_4$ without anions and solvents (plotted with Mercury 2.3).[75]

these complexes. The computed differences in first oxidation and reduction potentials are in good agreement with the experimental observations even for the $[Ru(tpy)(bpy)(halide)]^+$ complexes (Supporting Information Table S5,).[36]

A simple two state model as in Figure 1 leads to a second order secular equation, and the resulting expression for the absorption maximum is

$$h\nu_{max}(a) \approx [(E^{00'} + \lambda_{ex})^2 + 4(H_{DA})^2]^{1/2} \quad (3)$$

where H_{DA} is the normalized electronic matrix element for mixing the two electronic states. In the weak coupling limit ($\alpha^2_{DA} < 0.1$) this reduces to

$$h\nu_{max}(a) \approx E^{00'} + \lambda_{ex} + 2\alpha^2_{DA}(E^{00'} + \lambda_{ex}) + \ldots \quad (4)$$

where $E^{00'}$ is the minimum energy difference between the ground state and ^{1}MLCT excited state probed by absorption ($E^{0'0}$ is minimum energy difference between the lowest energy ^{3}MLCT excited state and the ground state), the mixing coefficient $\alpha_{DA} = H_{DA}/(E^{00'} + \lambda_{ex})$ and λ_{ex} is the excited state reorganizational energy (see Figure 1). To the extent that the differences in electrochemical oxidations and reductions are probes of the excited state energies (see the related discussion by Lever and Dodsworth),[64] the differences in the corresponding half-wave potentials can be represented as

$$-F\Delta E_{1/2} \approx E^{00'} + \Delta G_{solv(eq)} - T\Delta S_{vib(eq)} + 2\alpha^2_{DA}(E^{00'} + \lambda_{ex}) + \ldots \quad (5)$$

where ΔG_{solv} is the sum of the differences in free energies of solvation that accompany oxidation and reduction and ΔS_{vib} arises because the oxidized and reduced species have different vibrational frequencies and nuclear coordinates. Since ionic solvation energies are large,[65] $|\Delta G_{solv}|$ can be a substantial contribution (see also the discussion in Chen et al.).[16] Note that $\alpha^2_{DA}(E^{00'} + \lambda_{ex}) = \varepsilon_{DA}$ is the stabilization energy that results from D/A mixing in the coordinates of the ground state potential energy minimum. The chemical species involved in the optical and electrochemical processes are different, but they can be related by a simple electron transfer process of the form[16]

$$DA + D^+A^- \rightleftarrows D^+A + DA^- \quad (6)$$

The free energy contribution from eq 6 is approximately $[\Delta G_{solv(a)} - T\Delta S_{vib(a)} - \varepsilon_{AD} + \varepsilon_{DA}]$, where $\varepsilon_{AD} = \alpha^2_{DA}(E^{0'0} + \lambda_g)$ is the stabilization energy that results from D/A mixing in the coordinates of the lowest energy excited state potential energy minimum. Thus, for weakly coupled systems in which $E^{00'} \approx E^{0'0}$ and $\alpha^2_{DA}(\lambda_{ex} + \lambda_g) \ll E^{00'}$, eqs 4−6 can be combined to obtain the much used expression for optical-electrochemical correlations[16,64,66,67]

$$h\nu_{max}(a) \approx F\Delta E_{1/2} - \Delta G_{solv} + T\Delta S_{vib} + \lambda_{ex} + [\varepsilon_{DA} - \varepsilon_{AD}] + \ldots \quad (7)$$

While some problems with the general use and interpretation of eq 7 have been discussed in the literature,[16,64] it is a commonly employed experimental basis for assigning MLCT absorptions.[13,64,67,69]

The band I components that were deconvoluted from the low energy shoulders of the MLCT absorption envelope correlate

dx.doi.org/10.1021/ic2010387 |Inorg. Chem. 2011, 50, 11965–11977

Table 2. Coordination Sphere Bond Lengths [Å] for $[\{(tpy)(bpy)Ru\}_2CN](PF_6)_3\cdot(CH_3CN)_2$, $[Ru(bpy)_2\{NCRu(tpy)(bpy)\}_2](PF_6)_4$, $[Ru(tpy)(bpy)CN](PF_6)\cdot(CH_3CN)\cdot(H_2O)_{0.5}$, $[Ru(tpy)(bpy)I](PF_6)$, and $[Ru(tpy)(bpy)Br](PF_6)\cdot(C_4H_{10}O)_{0.5}$

		$[\{(L)Ru\}_2\text{-}CN](PF_6)_3\cdot(CH_3CN)_2$		$[Ru(bpy)_2\{NC\text{-}Ru(L)\}_2](PF_6)_4$			
		bond	length, Å	bond	length, Å	$[Ru(L)Br](PF_6)\cdot(C_4H_{10}O)_{0.5}$	
ligand, positions[a]		Ru(1) moiety		Ru(1) moiety		bond	length, Å
(bpy)	ax	Ru(1)−N(1)	2.078(2)	Ru(1)−N(1)	2.092(5)	Ru(1)−N(5)	2.031(6)
	eq	Ru(1)−N(2)	2.068(3)	Ru(1)−N(2)	2.084(5)	Ru(1)−N(4)	2.073(6)
(tpy)	t	Ru(1)−N(3)	2.069(2)	Ru(1)−N(3)	2.089(5)	Ru(1)−N(1)	2.068(7)
	c	Ru(1)−N(4)	1.969(3)	Ru(1)−N(4)	1.966(5)	Ru(1)−N(2)	1.948(6)
	t	Ru(1)−N(5)	2.068(3)	Ru(1)−N(5)	2.090(5)	Ru(1)−N(3)	2.049(7)
X		Ru(1)−N(11)	2.009(3)	Ru(1)−C(71)	1.982(6)	Ru(1)−Br(1)	2.5565(10)

		$[\{(L)Ru\}_2\text{-}CN](PF_6)_3\cdot(CH_3CN)_2$		$[Ru(bpy)_2\{NC\text{-}Ru(L)\}_2](PF_6)_4$			
		bond	length, Å	bond	length, Å	$[Ru(L)I](PF_6)$	
		Ru(2) moiety		Ru(3) moiety		bond	length, Å
(bpy)	ax	Ru(2)−N(6)	2.078(2)	Ru(3)−N(13)	2.097(5)	Ru−N(5)	2.053(2)
	eq	Ru(2)−N(7)	2.069(3)	Ru(3)−N(12)	2.063(6)	Ru−N(4)	2.103(2)
(tpy)	t	Ru(2)−N(8)	2.066(2)	Ru(3)−N(14)	2.065(6)	Ru−N(1)	2.073(2)
	c	Ru(2)−N(9)	1.956(3)	Ru(3)−N(15)	1.981(6)	Ru−N(2)	1.944(2)
	t	Ru(2)−N(10)	2.070(3)	Ru(3)−N(16)	2.079(6)	Ru−N(3)	2.067(2)
X		Ru(2)−C(51)	2.005(3)	Ru(3)−C(72)	1.992(6)	Ru−I	2.7257(3)

				$[Ru(bpy)_2\{NC\text{-}Ru(L)\}_2](PF_6)_4$			
		$[\{(L)Ru\}_2\text{-}CN](PF_6)_3\cdot(CH_3CN)_2$		bond	length, Å	$[Ru(L)CN](PF_6)\cdot(CH_3CN)\cdot(H_2O)_{0.5}$	
		bond	length, Å	Ru(2) moiety		bond	length, Å
(bpy)	ax[b]			Ru(2)−N(10)	2.044(5)	Ru−N(4)	2.087(3)
	eq[b]			Ru(2)−N(9)	2.054(5)	Ru−N(5)	2.108(3)
(bpy)				Ru(2)−N(7)	2.048(5)		
				Ru(2)−N(8)	2.047(5)		
(tpy)	t					Ru−N(3)	2.077(3)
	c					Ru−N(2)	1.960(3)
	t					Ru−N(1)	2.080(3)
X				Ru(2)−N(11)	2.026(5)	Ru−C(26)	2.006(4)
				Ru(2)−N(6)	2.036(5)		
(C−N)		N(11)−C(51)	1.155(4)	N(6)−C(71)	1.164(7)	N(6)−C(26)	1.147(5)
				N(11)−C(72)	1.151(7)		

[a] Pyridyl moiety positions with respect to the Ru−X bond for bpy: ax = coaxial and eq = equatorial; pyridyl positions within the equatorial tpy ligand: *t* = terminal; c = central. [b] Symbol of positions are not active for Ru(2) moiety of $[Ru(bpy)_2\{NC\text{-}Ru(L)\}_2]^{4+}$.

well with the differences in potentials for oxidations and reductions, as shown in Figure 3, while the dominant (band III) absorption maxima do not (Supporting Information, Figure S6).[36] To the extent that the electrochemical oxidation and reduction are probes of the energies of the HOMO(H-0) and LUMO(L+0), respectively, the correlation in Figure 3 indicates that the band I component of the MLCT absorption envelope arises from the H-0/L+0 transition; see also the computational results below. For the least-squares fit of the monometallic complexes ($r^2 = 0.90$; solid line in Figure 3): $h\nu_{max}$(H-0/L+0) = $(0.89 \pm 0.12)F\Delta E_{1/2} - 700 \pm 2400$ cm^{-1}; the observations for the $[\{(tpy)(bpy)Ru\}_2CN]^{3+}$ and $[(bpy)_2Ru\{CNRu(tpy)(bpy)\}_2]^{4+}$ complexes correlate well with those for the monometallic complexes (mean deviation 100 ± 50 cm^{-1}).

The use of the dominant absorption maximum, band III, results in a poorer correlation ($r^2 = 0.86$) with a slope of 0.60 ± 0.11 and intercept of 9300 ± 2000 cm^{-1} for the least-squares fit of the monometallic complexes, and the data for the multimetallic complexes deviate appreciably (900 ± 150 cm^{-1}; both complexes deviate from the line) from that correlation line.

B. X-ray Crystal Structures. X-ray crystal structures for $[Ru(tpy)(bpy)L]^{m+}$ have been reported previously for L = I,[68] pz,[29] and other ligands.[69−71] We have determined the X-ray crystal structures of $[Ru(tpy)(bpy)CN]^+$ and $[Ru(tpy)(bpy)Br]^+$ and repeated the $[Ru(tpy)(bpy)I]^+$ structure in the present work to make direct and internally consistent comparisons with the structures of the multimetallic complexes. Selected bond lengths

dx.doi.org/10.1021/ic2010387 |*Inorg. Chem.* 2011, 50, 11965–11977

Table 3. Coordination Sphere Bond Angles [deg] for $[\{(tpy)(bpy)Ru\}_2CN](PF_6)_3\cdot(CH_3CN)_2$, $[Ru(bpy)_2\{NC\text{-}Ru(bpy)(tpy)\}_2](PF_6)_4$, $[Ru(tpy)(bpy)CN](PF_6)\cdot(CH_3CN)\cdot(H_2O)_{0.5}$, $[Ru(tpy)(bpy)I](PF_6)$, and $[Ru(tpy)(bpy)Br](PF_6)\cdot(C_4H_{10}O)_{0.5}$ Complexes

	$[\{(L)Ru\}_2\text{-}CN](PF_6)_3$[a]		$[Ru(bpy)_2\{NC\text{-}Ru(L)\}_2](PF_6)_4$		$[Ru(L)CN](PF_6)$[a]	
structural components[b]	angle	degree	angle	degree	angle	degree
Ru−C−N	N(11)−C(51)−Ru(2)	169.7(3)	N(6)−C(71)−Ru(1)	173.5(5)	N(6)−C(26)−Ru	178.1(4)
			N(11)−C(72)−Ru(3)	172.8(6)		
C−N−Ru	C(51)−N(11)−Ru(1)	173.1(2)	C(71)−N(6)−Ru(2)	170.5(5)		
			C(72)−N(11)−Ru(2)	166.2(5)		
	Ru(1) moiety		*Ru(1) moiety*			
Ru-bpy	N(2)−Ru(1)−N(1)	78.20(10)	N(2)−Ru(1)−N(1)	77.53(19)	N(4)−Ru−N(5)	77.65(12)
T_c−Ru−T_t	N(4)−Ru(1)−N(5)	79.64(10)	N(4)−Ru(1)−N(3)	79.56(19)	N(2)−Ru−N(3)	79.60(12)
T_c−Ru−$T_{t'}$	N(4)−Ru(1)−N(3)	79.58(10)	N(4)−Ru(1)−N(5)	79.1(2)	N(2)−Ru−N(1)	79.23(13)
T_t−Ru−$T_{t'}$	N(5)−Ru(1)−N(3)	158.98(10)	N(3)−Ru(1)−N(5)	158.5(2)	N(3)−Ru−N(1)	158.82(13)
T_c−Ru−B_{eq}	N(4)−Ru(1)−N(2)	177.68(10)	N(4)−Ru(1)−N(2)	175.6(2)	N(2)−Ru−N(4)	173.01(12)
B_{ax}−Ru−T_t	N(3)−Ru(1)−N(1)	94.75(9)	N(3)−Ru(1)−N(1)	85.34(18)	N(3)−Ru−N(5)	91.69(12)
B_{ax}−Ru−$T_{t'}$	N(5)−Ru(1)−N(1)	86.24(10)	N(5)−Ru(1)−N(1)	95.6(2)	N(1)−Ru−N(5)	90.65(12)
B_{ax}−Ru−T_c	N(4)−Ru(1)−N(1)	101.54(10)	N(4)−Ru(1)−N(1)	100.41(19	*N(2)−Ru−N(5)*	*95.37(12)*
CN−Ru−B_{ax}	N(11)−Ru(1)−N(1)	173.59(10)				
B_{ax}−Ru−CN			C(71)−Ru(1)−N(1)	172.4(2)	C(26)−Ru−N(5)	171.81(14)
	Ru(2) moiety		*Ru(3) moiety*		$[Ru(L)Br](PF_6)$[a]	
Ru-bpy	N(7)−Ru(2)−N(6)	77.99(10)	N(12)−Ru(3)−N(13)	77.7(2)	N(5)−Ru(1)−N(4)	78.9(3)
T_c−Ru−T_t	N(9)−Ru(2)−N(8)	79.86(11)	N(15)−Ru(3)−N(14)	79.3(2)	N(2)−Ru(1)−N(3)	80.2(3)
T_c−Ru−$T_{t'}$	N(9)−Ru(2)−N(10)	79.77(11)	N(15)−Ru(3)−N(16)	79.2(3)	N(2)−Ru(1)−N(1)	79.7(3)
T_t−Ru−$T_{t'}$	N(8)−Ru(2)−N(10)	159.62(11)	N(14)−Ru(3)−N(16)	158.2(3)	N(3)−Ru(1)−N(1)	159.8(3)
T_c−Ru−B_{eq}	N(9)−Ru(2)−N(7)	176.02(10)	N(15)−Ru(3)−N(12)	172.8(2)	N(2)−Ru(1)−N(4)	177.3(3)
B_{ax}−Ru−T_t	N(10)−Ru(2)−N(6)	96.04(10)	N(14)−Ru(3)−N(13)	90.0(2)	N(5)−Ru(1)−N(3)	88.1(3)
B_{ax}−Ru−$T_{t'}$	N(8)−Ru(2)−N(6)	88.03(10)	N(16)−Ru(3)−N(13)	95.0(2)	N(5)−Ru(1)−N(1)	93.5(3)
B_{ax}−Ru−T_c	N(9)−Ru(2)−N(6)	99.87(10)	N(15)−Ru(3)−N(13)	95.4(2)	N(2)−Ru(1)−N(5)	98.6(3)
B_{ax}−Ru−CN	C(51)−Ru(2)−N(6)	174.99(12)	C(72)−Ru(3)−N(13)	173.4(2)		
B_{ax}−Ru−X					N(5)−Ru(1)−Br(1)	173.47(19)
			Ru(2) moiety		$[Ru(L)I](PF_6)$	
Ru-bpy			N(8)−Ru(2)−N(7)	79.2(2)	N(5)−Ru−N(4)	78.47(9)
			N(10)−Ru(2)−N(9)	79.2(2)		
bpy-Ru-bpy			N(8)−Ru(2)−N(9)	174.9(2)		
			N(10)−Ru(2)−N(8)	95.7(2)		
			N(7)−Ru(2)−N(9)	101.8(2)		
			N(10)−Ru(2)−N(7)	94.61(19)		
T_c−Ru−T_t					N(2)−Ru−N(1)	79.54(9)
T_c−Ru−$T_{t'}$					N(2)−Ru−N(3)	79.83(9)
T_t−Ru−$T_{t'}$					N(1)−Ru−N(3)	159.32(9)
T_c−Ru−B_{eq}					N(2)−Ru−N(4)	172.18(9)
B_{ax}−Ru−T_t					N(1)−Ru−N(4)	101.50(9)
B_{ax}−Ru−$T_{t'}$					N(5)−Ru−N(1)	88.88(9)
B_{ax}−Ru−T_c					N(5)−Ru−N(3)	93.86(9)
CN−Ru−B_{ax}			N(6)−Ru(2)−N(10)	173.8(2)		
			N(11)−Ru(2)−N(7)	175.5(2)		
B_{ax}−Ru−X					N(5)−Ru−I	174.28(6)

[a] Solvent molecules omitted. [b] Pyridyl moiety positions with respect to Ru−X bond for bpy (B): ax = coaxial and eq = equatorial; pyridyl positions within the equatorial tpy (T) ligand: t, t′ = terminal and c = central.

and bond angles of the structures (Figure 4) are presented in Tables 2 and 3. The remaining structural details can be found in the CIF files.[36]

The $[\{(tpy)(bpy)Ru\}_2CN]^{3+}$ structure is appreciably distorted. The distortion along the Ru−Ru axis is evident in Figure 5. Our computational modeling indicates that in the absence of lattice

dx.doi.org/10.1021/ic2010387 |*Inorg. Chem.* 2011, 50, 11965–11977

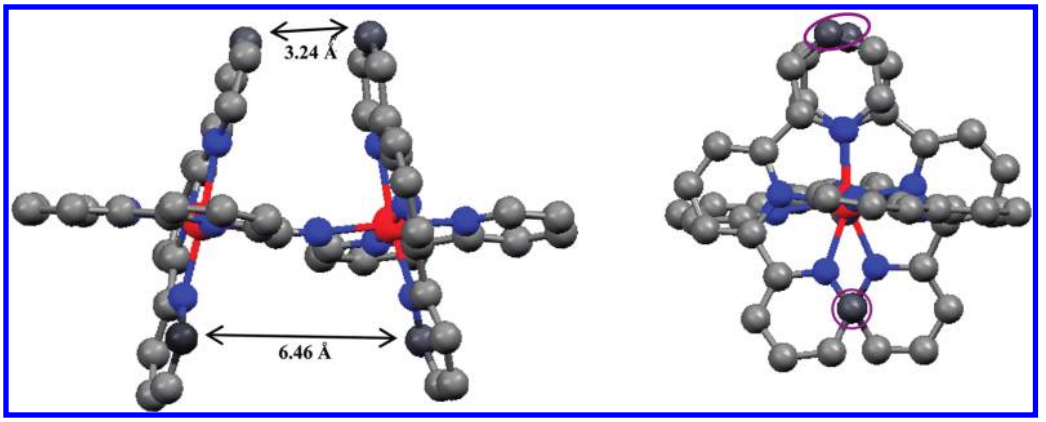

Figure 5. Views of the $[\{(tpy)(bpy)Ru\}_2CN]^{3+}$ complex orthogonal to (left) and along (right) the Ru−Ru axis (plotted by Mercury 2.3).[75] The C−C distances in the left view are between the darkened atoms which are circled in the axial view on the right.

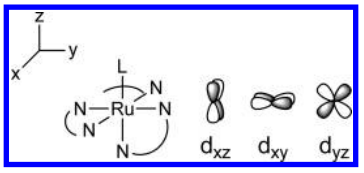

Figure 6. Cartoon of axis orientation and orbital labels.

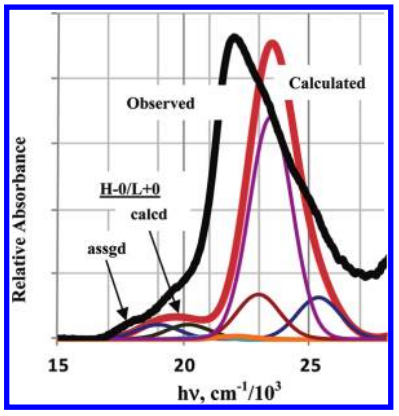

Figure 7. Comparison of observed (black) and calculated (red; B3PW91/SDDall/IEF-PCM) absorption spectra for $[Ru(tpy)(bpy)(CH_3CN)]^{2+}$. The calculated spectrum is a convolution of all the calculated component transitions (lighter lines) and H-0/L+0 designates the calculated (calcd) and assigned (assgd) Ru/tpy (H-0→L+0) transitions, respectively.

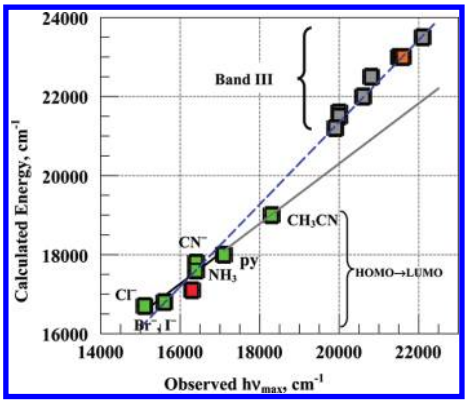

Figure 8. Comparison of observed and calculated MLCT absorption band components: The calculated HOMO→LUMO transition energies vs the band I contributions deconvoluted from the observed MLCT absorption envelopes, green and red; the calculated and observed absorption maxima for band III, gray and orange. The green and gray points are for the monometallic $[Ru(tpy)(bpy)L]^{m+}$ complexes (L indicated in the figure for the H-0→L+0 transitions) and the red and orange points are for $[\{(tpy)(bpy)Ru\}_2CN]^{3+}$. Uncertainties of ±200 cm^{-1} are rough estimates and are included for perspective. The least-squares line for the calculated H-0→L+0 and the lowest energy observed band maxima of the monometallic complexes (solid line; r^2 = 0.97): $h\nu_{max}$(calcd) = (0.76 ± 0.06)$h\nu_{max}$(obsd) + 5100 ± 1000 cm^{-1}. The least-squares fit to the calculated and observed, dominant MLCT absorption maxima of the monometallic complexes is (r^2 = 0.97): $h\nu_{max}$(calcd) = (1.0 ± 0.07)$h\nu_{max}$(obsd) + 1600 ± 1500 cm^{-1}. The combined data sets are fit by (r^2 = 0.99; blue dashed line in the figure): $h\nu_{max}$(calcd) = (1.04 ± 0.073)$h\nu_{max}$(obsd) + 550 ± 570 cm^{-1}.

constraints the equilibrium structure of $[\{(tpy)(bpy)Ru\}_2CN]^{3+}$ has the two tpy ligands in approximately parallel planes. Thus, while this distortion appears to be significant, it is likely to be the result of lattice interactions. Four of the PF_6^- anions lie approximately in a plane through the middle of the unit cell and nearly parallel to the unit cell *b*-axis while the other anions lie closer to the bpy ligands; it is likely that this asymmetry in the packing of anions and cations in the crystal lattice is a factor in the observed distortions. Even though it is unlikely that this structure is relevant to the electronic structures of solution species, our modeling (vide infra) suggests that the electronic structure is not significantly dependent on the conformation of Ru(tpy)(bpy) moieties around the M−(CN)−M axis anyway. The M−(CN) distortion mode is very weak (~100 cm^{-1})[72,73] and a wide range of M−(CN) bond angles has been reported,[74] so our solution measurements likely sample a variety of geometric structures.

There are some small structural differences between the complexes. The largest of these is about a 0.04 Å longer equatorial Ru−N(bpy) bond in the $[Ru(tpy)(bpy)CN]^+$ and $[Ru(tpy)(bpy)I]^+$ complexes than in the other complexes examined. The Ru−N and Ru−C bonds to the bridging cyanide differ more in length (2.03 and 1.99 Å, respectively) in the $[Ru(bpy)_2\{NC\text{-}Ru(bpy)(tpy)\}_2]^{4+}$ complex than in the $[\{(tpy)(bpy)Ru\}_2CN]^{3+}$ complex (2.007 ± 0.002 Å). We have

dx.doi.org/10.1021/ic2010387 |*Inorg. Chem.* 2011, 50, 11965–11977

Table 4. Calculated Compositions of the Lowest Energy MLCT Transitions of $[Ru(tpy)(bpy)L]^{m+}$ Complexes (B3PW91/SDDall/IEF-PCM)

		calculated (HOMO/LUMO)		observed
complex	transition	energy (cm^{-1})	oscillator strength (f)	energy (cm^{-1})
$[Ru(tpy)(bpy)Cl]^{+}$	H-0→L+0 (96%)	16,700	0.017	15,100
$[Ru(tpy)(bpy)I]^{+}$	H-0→L+0 (95%)	16,800	0.014	15,600
$[Ru(tpy)(bpy)NC]^{+}$	H-0→L+0 (97%)	17,100	0.017	
$[Ru(tpy)(bpy)NH_3]^{2+}$	H-0→L+0 (94%)	17,600	0.015	16,400
$[Ru(tpy)(bpy)CN]^{+}$	H-0→L+0 (94%)	17,800	0.012	16,400
$[Ru(tpy)(bpy)py]^{2+}$	H-0→L+0 (95%)	18,000	0.013	17,100
$[Ru(tpy)(bpy)CH_3CN]^{2+}$	H-0→L+0 (94%) H-1→L+0 (5%)	19,000	0.010	18300
$[\{(tpy)(bpy)Ru\}_2CN]^{3+}$ [a]	H-0→L+1 (73%) H-0→L+0 (14%)	17,000	0.014	16,300

[a] See also Table 5 below.

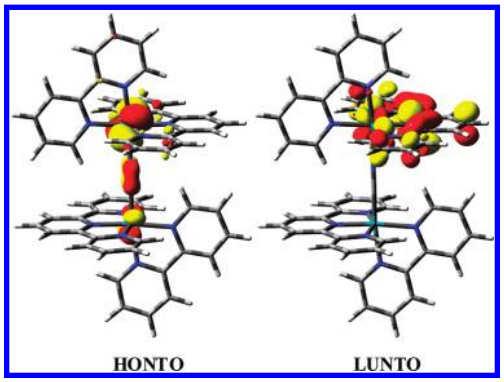

Figure 9. NTOs for the lowest energy MLCT transition in $[\{(tpy)(bpy)Ru\}_2CN]^{3+}$.

not found significant spectroscopic or computational effects that can be attributed to these structural differences.

C. Computational Results. The computed molecular orbitals and their (metal, ligand) compositions are presented in Supporting Information, Table S7.[36] For each of the monometallic Ru species we investigated, the first excited state was predominantly HOMO→LUMO in character. The HOMO was approximately Ru−d_{xz} (see Figure 6 for axis labels, with a slight tilt along the *x*-axis from *z* toward *y*) and the LUMO was tpy−π^* in character throughout the series. We attribute the relatively weak MLCT transition intensities of the first feature in the absorption spectra to poor spatial overlap of the HOMO and LUMO orbitals. In contrast, the Ru d_{xy} and d_{yz} orbitals overlap well with bpy−π^* (LUMO+1) and tpy−π^* (LUMO and LUMO+2) and this correlates with the greater intensity of band III.

The calculated spectra approximated the features of the observed lowest energy absorption profile reasonably well: The small oscillator strengths of the HOMO→LUMO and the HOMO→LUMO+1 components and their relationship to the dominant calculated features (band III) of the MLCT envelopes correlate well with the low energy shoulders observed in these complexes, Figures 7 and 8. However, the energies of the calculated absorption maxima were consistently too large by about 1300 ± 400 cm^{-1}; Figures 7, 8, Supporting Information, S6,[36] and Table 4. The higher energy, dominant absorption in this region (band III) is a convolution of several transitions generally involving the HOMO, HOMO-1, and HOMO-2 as donors and some combination of tpy and bpy acceptors; see Supporting Information, Table S5.[36]

The uncertainties in the deconvolutions or in assigning peak maxima may be larger than indicated in Figure 8 and the pertinent data are relatively few, but this figure indicates that the computational modeling (1) gives a reasonable approximation to the observed bandshapes, (2) supports the assignment of the lowest energy component of the shoulder of the MLCT absorption envelope as the H-0→L+0 transition, and (3) consistently overestimates the transition energies by approximately 10^3 cm^{-1}.

The band III component of the lowest energy MLCT absorption envelope is generally the result of the convolution of several different transitions and the dominant contributions to this absorption feature even change in their character with changes of the ancillary ligand (Supporting Information, S8).[36] Thus, the character of this higher-energy feature changes from Ru → tpy−π^* to Ru → bpy−π^* as L changes from π-donor (Cl^-, Br^-, I^-) to π-acceptor (MeCN, CN^-), with the σ-only donor NH_3 exhibiting charge transfer to both polypyridyl ligands. Band III is mostly due to transitions from the HOMO−1 orbital, and the ordering of d_{yz} and d_{xy} changes with the ligand field character of L because of stabilization (π-acceptor) and destabilization (π-donor) of the d_{yz} orbital. The ammine complex is an exception because the HOMO−1 and HOMO−2 orbitals are closer in energy, and both contribute to the absorption feature. This variation in the relative contributions to the dominant low energy MLCT absorption band at least partly accounts for the poor correlation found between this spectral feature and $F\Delta E_{1/2}$ (Supporting Information, S6).[36] Since these complexes contain two different acceptor ligands, the effects of such changes of provenance are no doubt larger for the $[Ru(tpy)(bpy)X]^{m+}$ complexes than in complexes with equivalent acceptors, but these observations do illustrate the inadvisability of quantitatively interpreting the slopes and/or intercepts of optical-electrochemical correlations when the spectral features used involve several components of different orbital composition.

The calculated transitions for the bimetallic-Ru complex are more complicated than those discussed above for the monometallic complexes. Thus, the lowest energy MLCT transition calculated for $[\{(tpy)(bpy)Ru\}_2CN]^{3+}$ is mostly HOMO→LUMO+1, but

dx.doi.org/10.1021/ic2010387 |*Inorg. Chem.* 2011, 50, 11965–11977

Table 5. Effects of Conformational Changes on the NTOs of $[\{(tpy)(bpy)Ru\}_2CN]^{3+}$ [a]

		HONTO				LUNTO		
		electronic density contribution from structural moiety				electronic density contribution from structural moiety		
structure	calculated (HONTO/LUNTO) absorption maximum, cm^{-1}	Ru^N (Ru^C)	tpy^N (tpy^C)	bpy^N (bpy^C)	CN	tpy^N	Ru^N	bpy^N
optimized structure	17000	66% (9%)	12% (2%)	5%	6%	90%	9%	
90 degree rotation[b]	17200	69% (7%)	12% (2%)	5%	5%	90%	9%	
180 degree rotation[b]	17100	66% (9%)	12% (2%)	5%	6%	90%	9%	
X-ray structure	17300	68% (7%)	14% (2%)	4%	5%	88%	9%	1%

[a] Fragment contributions were computed using a Mulliken population analysis. The superscripts "N" and "C" indicate the Ru-(NC) and Ru-(CN) moieties, respectively. [b] For rotation along the Ru−Ru axis.

this is still predominantly a Ru/tpy transition with the HOMO and LUMO+1 involving the Ru-(-NC) center and the adjacent tpy ligand. It was initially perplexing why the HOMO→LUMO transition is not lowest in energy, but this transition involves a Ru-(-NC) centered donor orbital and a tpy coordinated to the remote, Ru-(-CN) center acceptor orbital. Thus, this excited state involves opposite ends of the bimetallic species and incurs an energetic penalty due to larger charge separation than does the HOMO→LUMO+1 transition. Critically, the nearly isoenergetic LUMO and LUMO+1 orbitals make this charge separation penalty matter. To better represent the observed transition, we have computed the corresponding natural transition orbitals (NTO) which simplify the donor (HONTO) and acceptor (LUNTO) orbital contributions to the transition; these are shown in Figure 9 (see also Supporting Information, Table S10).[36] DFT has well-documented deficiencies for long-range charge transfer, so we verified these results with CAM-B3LYP.[76,77] The transition energy increases by ~4000 cm^{-1} going from B3PW91 to CAM-B3LYP for both the monometallic and bimetallic species, which suggests there is not an issue modeling the charge transfer state with B3PW91 (Supporting Information, Table S11).[36]

Since the X-ray structure involves a molecular conformation different from that of the optimized structure in Figure 9, we have examined the effects of molecular conformation on the HONTO/LUNTO electronic structures of the complex. The results, summarized in Table 5 and Supporting Information, S10,[36] indicate that simple conformational changes about Ru−C≡N−Ru do not significantly alter the excited state properties of $[\{(tpy)(bpy)Ru\}_2CN]^{3+}$.

DISCUSSION

That band I is observed for $[(bpy)_2Ru\{CNRu(tpy)(bpy)\}_2]^{4+}$ but not for its linkage isomer, $[(bpy)_2Ru\{NCRu(tpy)(bpy)\}_2]^{4+}$, demonstrates that this feature is a Ru^{II}/tpy MLCT transition. The systematic comparisons of experimental observations and the TD-DFT modeling studies of the MLCT absorption spectra show that similar weak, low energy features on the sides of the dominant, multicomponent absorption envelopes correspond to the H-0→L+0 transitions and are the chemically most relevant absorption components for the $[Ru(tpy)(bpy)L]^{m+}$ complexes. Closely related, weak and low energy absorptions that correspond to H-0→L+0 transitions have been previously found for the $[Ru(bpy)_2(L)_2]^{m+}$ and $[Ru(bpy)(L)_4]^{m+}$ complexes.[13] The small observed molar absorptivities of the absorption components corresponding to the HOMO→LUMO transitions in this series of complexes appear to arise from poor overlap of the donor and acceptor orbitals in the complexes.

The inference that $h\nu_{max}$(H-0/L+0) may be equal to or smaller than $F\Delta E_{1/2}$ initially seemed surprising, but it probably has a very simple explanation. Thus, ionic solvation free energies are very large and proportional to CZ^2/r_{eff} (where C is a constant of the order of a few thousand wavenumbers, Z is the ionic charge, and r_{eff} is the effective ionic radius) and the differences that result from oxidation ($Z\rightarrow Z+1$) and reduction ($Z\rightarrow Z-1$) combine to contribute $2C/r_{eff}$ to ΔG_{solv} in eqs 5 and 6. For example, a related solvational contribution to the half-wave potential of about +250 meV per unit of charge increase on the nearest neighbor metal M has been inferred previously for reductions of Ru^{III} centers in cyanide-bridged $[(L)M\{CN\text{-}(Ru^{III}(NH_3)_5\}_n]^{m+}$ complexes.[34] This effect amounts to a much larger net contribution of the solvational changes to electrochemical than the optical charge transfer process since the former involves a net change of charge while the latter only involves a change of dipole. This has to be a major contribution to the small or sometimes negative intercepts found in optical-electrochemical correlations. This is a much more obvious issue when H-0→L+0 transition energies are used in such correlations than when the higher energy absorption maxima are used. The reorganizational energy is the other major contribution to the intercept of these optical-electrochemical plots, but the decreases that are expected[18] for this contribution as $h\nu_{max}$(H-0→L+0)→0 may contribute to the decrease of the slope,[13,78] but they complicate the interpretation of the intercepts.

That the observed absorption bands assigned as H-0→L+0 transitions for the $[Ru(bpy)_2(L)_2]^{m+}$,[13] $[Ru(bpy)(L)_4]^{m+}$,[13] and $[Ru(tpy)(bpy)L]^{m+}$ complexes are all significantly smaller than the energy of the dominant maxima of the lowest energy MLCT absorption envelope has the important consequence that the difference in the energies of the H-0→L+0 absorptions and the observed energies of the maximum emission intensities (or emission maxima) are only a few thousand wavenumbers. Thus, the differences between the energies of the inferred ambient H-0→L+0 absorption maxima[13] and the 77 K emission maxima[11] reported for several $[Ru(bpy)_2X_2]^{m+}$ complexes average 3300 cm^{-1}, while our preliminary observations indicate that this difference is about half as large for the $[Ru(tpy)(bpy)X]^{m+}$ complexes (Supporting Information, Table S12).[36] This suggests that the effective reorganizational energies and/or electron exchange energies are small for these complexes. The small (and/or negative) intercepts of the optical-electrochemical plots

dx.doi.org/10.1021/ic2010387 |Inorg. Chem. 2011, 50, 11965–11977

(Figure 3 and preceding paragraph) are related to this inference in that they imply small reorganizational energies. This issue is being further investigated.

The H-0→L+0 transition generates Ru^{II}/Ru^{III} mixed valence excited states in the $[\{(tpy)(bpy)Ru\}_2CN]^{3+}$ and $[(bpy)_2Ru\{CNRu(tpy)(bpy)\}_2]^{4+}$ complexes. The observations in Table 1 indicate that the ground state stabilization energy that results from this electronic delocalization is about 1600 cm^{-1} per nearest neighbor Ru^{II}/Ru^{III} center (based on the effect of substituting Rh^{III} for Ru^{II}; see also Lin, et al.).[79] Since the complexes with mixed valence excited states correlate well ($\pm\sim$ 400 cm^{-1}) with the monometallic complexes in Figure 3, the stabilization energy that results from Ru^{III}/Ru^{II} electronic delocalization must make comparable contributions to the optical transition energy and to the electrochemical oxidations. However, the computational modeling suggests that a significant fraction of the charge is delocalized in the Franck−Condon excited state from a terminal Ru^{III} to the cyanide ligand in both $[\{(tpy)(bpy)Ru\}_2CN]^{3+}$ and $[Ru(tpy)(bpy)CN]^{+}$, with that fraction being slightly larger for the latter. Furthermore, the net positive charge delocalized onto the other, nominally Ru^{II}-center of the bimetallic complex appears to be only twice as large as that onto cyanide (Tables 5 and Supporting Information, S7).[36] The net electronic delocalization across the Ru−(CN)−Ru axis in the $[\{(tpy)(bpy)Ru\}_2CN]^{3+}$ mixed valence excited state appears to be about 20%, and the effects of this delocalization are not easily described using the conventional treatment of mixed valence complexes.[79,80] Furthermore, it is interesting that the calculated ratios of electronic density on the coordinated tpy ligands to that on their respective Ru centers is about 15−20% for both Ru(tpy) moieties (see Table 5).

The weak contributions corresponding to H-0→L+0 transitions make it very difficult to obtain useful experimental information about the lowest energy electronic excited states from absorption spectra: (a) the identification of these contributions to the absorption spectra must be substantiated with other experimental and/or theoretical information; (b) the use of absorption bands other than those corresponding to the H-0→L+0 transitions can lead to errors in inferences about excited state properties. For example, for the complexes considered here the use of the dominant low energy MLCT absorption feature in comparisons to electrochemical observations would lead to errors in the correlation slopes and intercepts and consequently misleading evaluations of such properties as the net configurational mixing with the ground state, reorganizational energies and/or exchange energies.

■ ASSOCIATED CONTENT

Ⓢ Supporting Information. CIF files; selected crystal data and structure refinement; absorption spectra of $[R(tpy)(bpy)L]^{m+}$ complexes; electrochemistry and absorption spectra of multimetal complexes containing Ru(II) and Ru(III); electrochemistry of $[Ru(tpy)(bpy)X]^{+}$ complexes; computational modeling of half-wave potentials; spectral/electrochemical correlation for the dominant low energy MLCT absorption band; Mulliken population analysis; calculated orbital compositions; comparison of observed and calculated spectra; NTOs computed for $[\{(tpy)(bpy)Ru\}_2CN]^{3+}$; comparison of B3PW91 and CAM-B3LYP energies; comparison of absorption and emission maxima of some Ru-polypyridyl complexes. This material is available free of charge via the Internet at http://pubs.acs.org.

■ AUTHOR INFORMATION

Corresponding Author

*E-mail: 054971@mail.fju.edu.tw (Y.-J.C.), jfe@chem.wayne.edu (J.F.E).

■ ACKNOWLEDGMENT

This work was funded in part (Y.-J.C.) by the National Science Council of the R.O.C. through Grants NSC-95-2113-M-030-003 and NSC-96-2113-M-030-006-MY2 and in part (J.F.E. and H.B.S.) by the Division of Chemical Sciences, Geosciences, and Biosciences, Office of Basic Energy Sciences of the U.S. Department of Energy through Grant DE-FG02-09ER16120.

■ REFERENCES

(1) Myers, A. B. *Chem. Rev.* **1996**, *96*, 911.
(2) Myers, A. B. *Acc. Chem. Res.* **1997**, *30*, 519.
(3) Hupp, J. T.; Williams, R. T. *Acc. Chem. Res.* **2001**, *34*, 808.
(4) Maruszewski, K.; Bajdor, K.; Strommen, D. P.; Kincaid, J. R. *J. Phys. Chem.* **1995**, *99*, 6286.
(5) Thompson, D. G.; Schoonover, J. R.; Timpson, C. J.; Meyer, T. J. *J. Phys. Chem. A* **2003**, *107*, 10250.
(6) McCusker, J. K. *Acc. Chem. Res.* **2003**, *36*, 876.
(7) *Electron Transfer in Chemistry*; Balzani, V., Ed.; Wiley-VCH: Weinheim, Germany, 2001; Vols. 1−5.
(8) Marcus, R. A. *Annu. Rev. Phys. Chem.* **1964**, *15*, 155.
(9) Bryant, G. M.; Ferguson, J. E.; Powell, H. K. *Aust. J. Chem.* **1971**, *24*, 257.
(10) Koiwa, T.; Masuda, Y.; Shono, J.; Kawamoto, Y.; Hoshino, Y.; Hashimoto, T.; Natarajau, K.; Shimizu, K. *Inorg. Chem.* **2004**, *43*, 6215.
(11) Odongo, O. S.; Heeg, M. J.; Chen, J. Y.; Xie, P.; Endicott, J. F. *Inorg. Chem.* **2008**, *47*, 7493.
(12) Kalinina, D.; Dares, C.; Kaluarachchi, H.; Potvin, P. G.; Lever, A. B. P. *Inorg. Chem.* **2008**, *47*, 10110.
(13) Allard, M. M.; Odongo, O. S.; Lee, M. M.; Chen, Y.-J.; Endicott, J. F.; Schlegel, H. B. *Inorg. Chem.* **2010**, *49*, 6840.
(14) Gorelsky, S. I.; Lever, A. B. P.; Ebadi, M. *Coord. Chem. Rev.* **2002** *230*, 97.
(15) Sarkar, B.; Patra, S.; Fiedler, J.; Sunoj, R. B.; Janardanan, D.; Lahiri, G. K.; Kaim, W. *J. Am. Chem. Soc.* **2008**, *130*, 3532.
(16) Chen, Y.-J.; Endicott, J. F.; Swayambunathan, V. *Chem. Phys.* **2006**, *326*, 79.
(17) Odongo, O. S.; Endicott, J. F. *Inorg. Chem.* **2009**, *48*, 2818.
(18) Xie, P.; Chen, Y.-J.; Uddin, M. J.; Endicott, J. F. *J. Phys. Chem. A* **2005**, *109*, 4671.
(19) Endicott, J. F.; Chen, Y.-J. *Coord. Chem. Rev.* **2007**, *251*, 328.
(20) Endicott, J. F.; Schegel, H. B.; Uddin, M. J.; Seneviratne, D. *Coord. Chem. Rev.* **2002**, *229*, 95.
(21) Tseng, H.-W.; Zong, R.; Muckerman, J. T.; Thummel, R. *Inorg. Chem.* **2008**, *47*, 11763.
(22) Seok, W. R.; Meyer, T. J. *Inorg. Chem.* **2005**, *44*, 3931.
(23) Meyer, T. J.; Huynh, M. H. V. *Inorg. Chem.* **2003**, *42*, 8140.
(24) Keene, F. R.; Adcock, P. A.; Smythe, R. S.; Snow, M. R. *Inorg. Chem.* **1984**, *23*, 2336.
(25) Pennington, W. T.; Petersen, J. D.; Billadeau, M. A. *Acta Crystallogr.* **1990**, *C46*, 1105.
(26) Curtis, J. C.; Yang, J.; Seneviratne, D.; Arbatin, G.; Andersson, A. M. *J. Am. Chem. Soc.* **1997**, *119*, 5329.
(27) Keene, F. R.; Ridd, M. J. *J. Am. Chem. Soc.* **1981**, *103*, 5733.
(28) McMillin, D. R.; Hecker, C. R.; Fanwick, P. E. *Inorg. Chem.* **1991**, *30*, 659.
(29) Gulyas, P. T.; Hambley, T. W.; Lay, P. A. *Aust. J. Chem.* **1996**, *49*, 527.

(30) Watzky, M. A. Ph.D. Dissertation, Wayne State University, Detroit, Michigan, 1994.
(31) *IGOR Pro 6.2.1.0*; Wavemetrics, Inc.: Lake Oswego, OR, 2010.
(32) Gennett, T.; Milner, D. F.; Weaver, M. J. *J. Phys. Chem.* **1985**, *89*, 2787.
(33) Bard, A. J.; Faulkner, L. R. *Electrochemical Methods*; Wiley: New York, 1980.
(34) Watzky, M. A.; Macatangay, A. V.; Van Camp, R. A.; Mazzetto, S. E.; Song, X.; Endicott, J. F.; Buranda, T. *J. Phys. Chem. A* **1997**, *101*, 8441.
(35) Sheldrick, G. M. *SHELXTL-97*; Bruker Analytical X-ray Systems, Inc.: Madison,WI, 1997.
(36) See Supporting Information.
(37) Parr, R. G.; Yang, W. *Density-functional theory of atoms and molecules*; Oxford University Press: New York, 1989.
(38) Frisch, M. J.; Trucks, G. W.; Schlegel, H. B.; Scuseria, G. E.; Robb, M. A.; Cheeseman, J. R.; Scalmani, G.; Barone, V.; Mennucci, B.; Nakatsuji, G. A. P. H.; Caricato, M. L., X.; Hratchian, H. P.; Izmaylov, A. F.; Bloino, J. Z.,G.; Sonnenberg, J. L.; Hada, M.; Ehara, M.; Toyota, K.; Fukuda, R.; Hasegawa, J.; Ishida, M.; Nakajima, T.; Honda, Y.; Kitao, O.; Nakai, H.; Vreven, T. J. A.; Montgomery, J.; Peralta, J. E.; Ogliaro, F.; Bearpark, M.; Heyd, J. J.; Brothers, E.; Kudin, K. N.; Staroverov, V. N.; Keith, T.; Kobayashi, R.; Normand, J.; Raghavachari, K.; Rendell, A.; Burant, J. C.; Iyengar, S. S.; Tomasi, J.; Cossi, M.; Rega, N.; Millam, J. M.; Klene, M.; Knox, J. E.; Cross, J. B.; Bakken, V.; Adamo, C.; Jaramillo, J.; Gomperts, R.; Stratmann, R. E.; Yazyev, O.; Austin, A. J.; Cammi, R.; Pomelli, C.; Ochterski, J. W.; Martin, R. L.; Morokuma, K.; Zakrzewski, V. G.; Voth, G. A.; Salvador, P.; Dannenberg, J. J.; Dapprich, S.; Parandekar, P. V.; Mayhall, N. J.; Daniels, A. D.; Farkas, O.; Foresman, J. B.; Ortiz, J. V.; Cioslowski, J.; Fox, D. J. *Gaussian Development Version*, Revision H.09+; Gaussian Inc.: Wallingford, CT, 2010.
(39) Becke, A. D. *J. Chem. Phys.* **1993**, *98*, 5648.
(40) Krishnan, R.; Binkley, J. S.; Seeger, R.; Pople, J. A. *J. Chem. Phys.* **1980**, *72*, 650.
(41) Perdew, J. P. *Phys. Rev. B* **1986**, *33*, 8822.
(42) Perdew, J. P.; Burke, K.; Wang, Y. *Phys. Rev.* **1996**, *54*, 16533.
(43) Andrae, D.; Haussermann, U.; Dolg, M.; Stoll, H.; Preuss, H. *Theor Chim Acta* **1990**, *77*, 123.
(44) Dunning, T. H., Jr.; Hay, P. J. In *Modern Theoretical Chemistry*; Schaefer, H. F., III, Ed.; Plenum: New York, 1976; Vol. 3, p 1.
(45) Igelmann, G.; Stoll, H.; Preuss, H. *Mol. Phys.* **1988**, *65*, 1321.
(46) Schlegel, H. B.; McDouall, J. J. In *Computational Advances in Organic Chemistry*; Ögretir, C., Csizmadia, I. G., Eds.; Kluwer Academic: Amsterdam, The Netherlands, 1991.
(47) Bauernschmitt, R.; Ahlrichs, R. *J. Chem. Phys.* **1996**, *104*, 9047.
(48) Schlegel, H. B. *J. Comput. Chem.* **1982**, *3*, 214.
(49) Miertuš, S.; Scrocco, E.; Tomasi, J. *Chem. Phys.* **1981**, *55*, 117.
(50) Tomasi, J.; Mennucci, B.; Cammi, R. *Chem. Rev.* **2005**, *105*, 2999.
(51) Scalmani, G.; Frisch, M. J.; Mennucci, B.; Tomasi, J.; Cammi, R.; Barone, V. *J. Chem. Phys.* **2006**, *124*, 094107.
(52) Scalmani, G.; Frisch, M. J. *J. Chem. Phys.* **2010**, *132*, 114110.
(53) Runge, E.; Gross, E. K. U. *Phys. Rev. Lett.* **1984**, *52*, 997.
(54) Stratmann, R. E.; Scuseria, G. E.; Frisch, M. J. *J. Chem. Phys.* **1998**, *109*, 8218.
(55) Petit, L.; Maldivi, P.; Adamo, C. *J. Chem. Theory Comput.* **2005**, *1*, 953.
(56) Gorelsky, S. I.; http://www.sg-chem.net/, 2009.
(57) Pennington, R.; Keith, T.; Millam, J. M. *GaussView*; Semichem, Inc.: Shawnee Mission, KS, 2009.
(58) Baik, M.-H.; Friesner, R. A. *J. Phys. Chem. A* **2002**, *106*, 7407.
(59) Roy, L. E.; Jakubikova, E.; Guthrie, M. G.; Batista, E. R. *J. Phys. Chem. A* **2009**, *113*, 6745.
(60) Cohen, A. J.; Mori-Sánchez, P.; Yang, W. *Science* **2008**, *321*, 792.
(61) Nozaki, K.; Takamori, K.; Nakatsugawa, Y.; Ohno, T. *Inorg. Chem.* **2006**, *45*, 6161.
(62) Martin, R. L. *J. Chem. Phys.* **2003**, *118*, 4775.
(63) Jakubikova, E.; Chen, W.; Dattelbaum, D. M.; Rein, F. N.; Rocha, R. C.; Martin, R. L.; Batista, E. R. *Inorg. Chem.* **2009**, *48*, 10720.
(64) Lever, A. B. P.; Dodsworth, E. S. In *Electronic Structure and Spectroscopy of Inorganic Compounds*, Vol. II; Lever, A. B. P., Solomon, E. I., Eds.; Wiley: New York, 1999; p 227.
(65) Phillips, C. S. G.; Williams, R. J. P. *Inorganic Chemistry*; Oxford University Press: New York, 1965; Vol. I.
(66) Caspar, J. V.; Meyer, T. J. *Inorg. Chem.* **1983**, *22*, 2446.
(67) Dodsworth, E. S.; Lever, A. B. P. *Chem. Phys. Lett.* **1986**, *124*, 152.
(68) Billadeau, M. A.; Pennington, W. T.; Petersen, J. D. *Acta Crystallogr.* **1990**, *C46*, 1105.
(69) Adcock, P. A.; Keene, F. R.; Smythe, R. S.; Snow, M. R. *Inorg. Chem.* **1984**, *23*, 2336.
(70) Yang, X.-J.; Drepper, F.; Wu, B.; Sun, W.-H.; Haehnelb, W.; Janiak, C. *Dalton Trans.* **2005**, 2 5 6.
(71) Al-Noaimi, M.; Yap, G. P. A.; Crutchley, R. J. *Inorg. Chem.* **2004**, *43*, 1770.
(72) Flint, C. D. *J. Chem. Soc., Faraday Trans. II* **1976**, *72*, 721.
(73) Flint, C. D.; Greenough, P. *J. Chem. Soc., Faraday Trans. II* **1974**, *70*, 815.
(74) Lessard, R. B.; Heeg, M. J.; Buranda, T.; Perkovic, M. W.; Schwarz, C. L.; Rudong, Y.; Endicott, J. F. *Inorg. Chem.* **1992**, *31*, 3091.
(75) *Mercury 2.3*; The Cambridge Crystallographic Data Centre: Cambridge, U.K., 2011.
(76) Dreuw, A.; Head-Gordon, M. *Chem. Rev.* **2005**, *105*, 4009.
(77) Yanai, T.; Tew, D. P.; Handy, N. C. *Chem. Phys. Lett.* **2004**, *393*, 51.
(78) Odongo, O. S.; Allard, M. M.; Schlegel, H. B.; Endicott, J. F. *Inorg. Chem.* **2010**, *49*, 9095.
(79) Tsai, C.-N.; Huang, S.-Y.; Endicott, J. F.; Chen, Y.-J.; Chen, H.-Y. *Inorg. Chem.* **2011**, *50*, 8274.
(80) Hush, N. S. *Prog. Inorg. Chem.* **1967**, *8*, 391.

NOTE ADDED AFTER ASAP PUBLICATION

This paper published on the Web on November 8, 2011, without the CIF file. The corrected version was reposted on November 28, 2011.